sensors

Article

A roadmap for Gigabit to Terabit optical wireless communications receivers

William Matthews [1] and Steve Collins[2,*]

[1] Department of Engineering Science, University of Oxford; william.matthews@eng.ox.ac.uk
[2] Department of Engineering Science, University of Oxford; steve.collins@eng.ox.ac.uk
* Correspondence: steve.collins@eng.ox.ac.uk

Abstract: Silicon photomultiplier's relatively large area and ability to detect single photons makes them attractive as receivers for optical wireless communications. In this paper the relative importance of the non-linearity and the width of the SiPMs fast output on their performance in receivers are investigated using Monte Carlo simulations. Using these results the performance of receivers containing different SiPMs is estimated. This is followed by discussion of the potential performance of arrays of existing SiPMs. Finally, the possible dramatic improvements in performance that could be achieved by using two stacked integrated circuits is highlighted.

Keywords: Visible Light Communications, Optical Wireless Communications, SiPM, Monte Carlo Simulations

Citation: To be added by editorial staff during production.

Academic Editor: Firstname Lastname

Received: date
Accepted: date
Published: date

1. Introduction

Optical wireless communications (OWC) and visible light communications (VLC) systems are being investigated as a way to increase local wireless communications capacity [1]. An important performance parameter for any communications system is the bit error rate (BER), which depends upon the signal to noise ratio (SNR) at the receiver's output. An approach to increasing the SNR of an OWC or VLC system is to use silicon photomultipliers (SiPMs) in the receiver [2-18]. These devices are arrays of microcells, containing a single photon avalanche diode (SPAD), that are designed so that an output pulse is generated whenever an avalanche event occurs. Since a single photon can initiate an avalanche these microcells can detect individual photons. It is this ability to detect photons which means that the sensitivity of a SiPM receiver is expected to be limited by Poisson statistics.

When on-off keying (OOK) is used the number of detected photons per bit when a zero is received determines the average number of photons per bits required to achieve a particular BER. Since avalanche events can be initiated in the dark, at a rate known as the dark count rate (DCR), existing SiPMs are particularly suited to data rates of more than 100 Mbps. Consequently, SiPM receivers have been shown to operate within a few photons per bit of the noise floor determined by Poisson statistics [5]. Unfortunately, after a microcell has detected a photon the avalanche event has to be quenched by reducing the voltage across the avalanche photodiode (APD) in the microcell. The microcell then has to be recharged and this means that the SiPM has a non-linear response [4].

The performance of receivers containing commercially available SiPMs can be determined experimentally [3-7, 9-18]. Ideally, the results of these experiments could be used to inform the selection of the best SiPMs from amongst those that have different characteristics. Unfortunately, the transmitter can have a significant impact on any experimental results. Furthermore, it can be very difficult to separate the impact of the SiPMs bandwidth and its non-linear response. Recently, these problems led to the development of a Monte Carlo simulator [19]. The parameters in this simulator were obtained from either the relevant data sheet or experimental results. Then the results of the simulator were validated by comparing them to results of experiments into the impact of ambient light on the performance of receivers [19].

The aim of this paper is to use this Monte Carlo simulator to compare the impact of the SiPMs non-linearity and bandwidth on their performance in receivers. The results of this comparison are then used to estimate the performance of commercially available SiPMs when the data is represented by OOK. Guidelines on the selection of SiPM for use in receivers have been published previously [20, 21]. However, both of these papers assumed that the modulation scheme was orthogonal frequency division multiplexing (OFDM) which isn't as energy efficient as OOK [22]. Furthermore, it was assumed that it is possible to increase the area of the SiPM without changing any other parameters. In contrast, this paper concentrates upon OOK. In addition, the data sheets of SiPMs show that increasing the area of a SiPM has a significant negative impact on the width of the SiPM's fast output pulses and hence its bandwidth. Fortunately, there is a method of combining SiPMs so that they act in parallel but retain their bandwidth. The results of the simulation are therefore used to investigate the impact of using multiple SiPMs in parallel in a receiver. Finally, a review of the recently developed technology leads to the conclusion that using two stacked integrated circuits to make SiPMs will dramatically increase the data rates that can be supported.

This paper is organized as follows. Section 2 contains a list of the important characteristics of commercially available SiPMs. This is followed by a brief justification of some assumption made when constructing the Monte Carlo simulator and a description of the small changes that have been made to the simulator previously reported in detail [19]. Section 3 then starts with a discussion of the BER of an OOK signal when the number of detected photons per bit is determined by Poisson statistics. This section also contains evidence that the equation that represents the SiPM non-linearity, previously observed in the presence of ambient light, is also relevant when high irradiances are used to transmit OOK data. Finally, the section contains a discussion of inter-symbol interference (ISI) caused by the SiPMs output pulses and the resulting increase in the rate at which photons need to be detected at different data rates. Section 4 then contains a discussion of the impact of the SiPMs non-linearity and the width of SiPM's fast output pulses. This discussion includes a suggested method of determining the data rate at which each of these phenomena will become important for each SiPM. However, results show that SiPMs with a high maximum count rate can support data rates that are significantly higher than these two data rates. A method which allows SiPMs to be used in parallel, and the possible consequences of using this method, are then discussed. This is followed by a discussion of the possible advantages of using 850 nm transmitters rather than 405 nm transmitters. The possible performance of a stacked receiver is then discussed. Finally section 5 contains some conclusions from this work.

2. Materials and Methods

2.1 Characteristics of Commercially available SiPMs

SiPMs are available from AdvanSiD, Broadcomm, First Sensor, Hamamatsu and onsemi. All these manufacturers supply SiPMs that contain arrays of microcells, with each microcell containing an APD in series with a resistor. These microcells are connected in parallel and biased above the breakdown voltage of the APDs. This means that if a photon initiates an avalanche event in a microcell the resulting current causes a voltage drop across the resistor. The resulting reduction in the voltage across the APD then quenches the avalanche event. The capacitance within the microcell is then recharged until the bias voltage

Table 1 Key parameters for the three series of commercially available SiPMs manufactured by onsemi [23-25]

Name	Area (mm^2)	Pitch (μm)	Number of μcells	Recovery Time (ns)	Maximum Count Rate (Gcps)	PDE at 405nm	Fast Output Pulse Width (ns)
RB10010	1	10	4296	12	162.7	0.1	2.3
RB10020	1	20	1590	21	34.4	0.11	2
RB10035	1	35	620	73	3.9	0.12	3.7
C10010	1	10	2880	5	261.8	0.17	0.6
C10020	1	20	1296	23	25.6	0.29	0.6
C10035	1	35	504	82	2.8	0.39	0.6
C30020	9	20	10998	23	217.4	0.29	1.5
C30035	9	35	4774	82	26.5	0.39	1.5
C30050	9	50	2668	159	7.6	0.44	1.5
C60035	36	35	18980	95	90.8	0.39	3.2
J30020	9	20	14410	15	436.7	0.38	1.4
J30035	9	35	5676	45	57.3	0.46	1.5
J40035	16	35	9260	48	87.7	0.46	1.7
J60035	36	35	22292	50	202.7	0.46	3

across the APD is restored. During this recovery time the microcells ability to detect photons is reduced [19]. Consequently, the need to recharge the microcells creates a non-linear SiPM response [19]. An important difference when selecting SiPMs for receivers is that onsemi creates an output which is capacitively coupled to each microcell. It is this capacitive coupling that creates fast output pulses on this second output. These narrower, fast output pulses are typically an order of magnitude narrower than the output pulses on other SiPMs. Since this significantly reduces ISI at higher data rates the SiPMs from onsemi have often been used to create receivers [5-7, 10-18].

Onsemi produce three series of SiPMs. The C and J series are manufactured on p-on-n substrates [26] and have a peak PDE at approximately 425 nm. The difference between these two series is that the J series use a through silicon via (TSV) process to minimize the dead space between microcells. In addition, onsemi produce the RB series of SiPMs. Unlike the other two series the RB SiPMs are manufactured using an n-on-p substrate [26]. This change in substrate means that the RB devices have a peak PDE at approximately 600 nm. The important parameters for the RB, C and J series SiPMs sold by onsemi were obtained from the relevant data sheets and are listed in Table 1. In this table the PDE at 405 nm has been listed because this is the wavelength that has been used to reduce the impact of ambient irradiance from white LEDs [12].

The data for the C and J series devices with the same area and microcell size, for example the J30035 and C30035, shows that the TSV process increases the SiPM PDE and number of microcells and significantly reduces its recovery time. This means that when the transmitter operated at 405 nm the J series has been favored [5-7, 10-12, 14-15, 17-18].

As expected, within any series of SiPMs reducing the microcell size increases the number of microcells per unit area. However, the data in Table 1 shows that it also reduces the PDE. The higher PDE of the larger microcells is an obvious advantage. However, the need to recharge microcells after quenching creates a non-linear response. This means that at higher photon count rates a larger number of microcells will be more important than the PDE. The best choice of microcell size will therefore depend upon the expected count rate of photons.

Most importantly, in free space, a transmitter generates particular irradiances at different relative locations [12]. The irradiance required to support a particular data rate and BER is therefore the most important performance metric for free space receivers. For any irradiance a larger SiPM will detect more photons from the transmitter. Using a larger area should therefore improve the receiver's performance. However, the data in Table 1 shows that increasing the area of a SiPM also increases its fast output pulse width. This means that smaller SiPMs are expected to be able to operate at higher data rates before their output pulses cause ISI. The trade-off in pairs of characteristics such as number of microcells per unit area and PDE or SiPM area and fast output pulse width have been investigated by numerical simulations.

2.2 Numerical Simulations

Numerical simulations have been performed using a Monte Carlo simulator described in detail previously [19]. This simulator doesn't include the effects of dark counts, after-pulsing and optical cross-talk. Previously, it was shown that omitted these phenomena from the simulator didn't impact the ability to predict the impact of ambient light on a SiPM [19]. These phenomena have not been added to the current simulation. In the case of the dark counts this is because, for data rates of 1 Gbps or higher, the dark count rates of the simulated SiPMs are negligible compared to the rate at which photons are detected [19]. Similarly, for the SiPMs that are simulated both the after-pulsing probability and the probability of optical cross-talk are less than 10%. These phenomena might therefore increase the irradiance falling on a SIPM required to achieve a particular performance by up to 10%. However, this is a small increase compared to the impact of the non-linearity and finite pulse width that are the subject of the current study.

The original implementation of the simulator was used to investigate the impact of ambient light. This meant that photons were detected when a zero was received. In contrast, the simulations in this paper assume that the SiPM has been protected from ambient light using a filter. This means that when a zero is received the dominant noise source is the noise from the electronics, for example the RF amplifier, in the receiver. After amplification the peak-to-peak voltage for a single avalanche event in a J 30020 SiPM was 15 mV_{PP}. Whilst, when the beam from the transmitter is blocked a 5 mV_{PP} (three standard deviations) white noise signal was observed. For the simulations whose results are reported in this paper Gaussian white noise with a peak-to-peak amplitude of one third of the peak-to-peak amplitude of an avalanche event was added to the output of the simulator before decoding.

3. Results

3.1. Poisson Statistics and BER

The dominant noise source in a SiPM receiver is expected to be Poisson noise. If this is the case and an OOK signal is transmitted the BER can be calculated using [6]

$$\mathbf{BER} = \frac{1}{2}\left[\sum_{k=0}^{n_T} \frac{(N_{Tx}+N_b)^k}{k!} . e^{-(N_{Tx}+N_b)} + \sum_{k=n_T}^{\infty} \frac{(N_b)^k}{k!} . e^{-N_b}\right] \quad (1)$$

where N_{Tx} is the number of additional detected photons per bit whena one is received and N_b is the average number of photons detected per bit time when a zero is received.

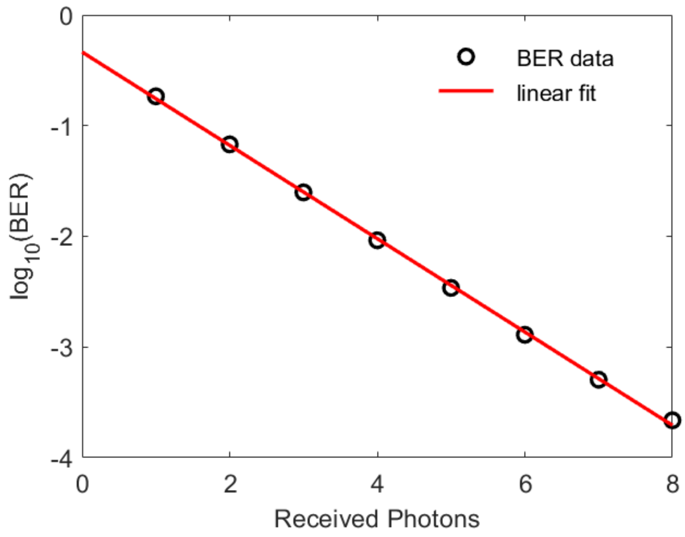

Figure 1 The number of recieved photons required to represent a logic one, N_{Tx}, to achieve a range of BERs when $\mathrm{N_b} = 0$. The range of BERs shown is close to the value of 3.8×10^{-3} needed when forward error correction is used to significantly reduce the final BER. The results obtained with different integer number of additional photons are shown as black circles. The red line is then a linear fit to the points.

In addition n_T is the threshold used to differentiate a zero from a one. The value of n_T that is used is the value which minimizes the BER.

One important consequence of equation (1) is demonstrated in Fig 1. The results in this figure show that the BER is very sensitive to the number of detecting photons per bit. In addition, this figure shows a linear fit to the relationship between the BER and N_{Tx} obtained using the linear fitting tool in MATLAB. This fit means that, at least in this range of BERs, the relationship between BER, BER, and , N_{Tx}, is

$$N_{Tx} = -\left(log_{10}(BER) + 0.33\right)/0.42 \tag{2}$$

The relationship between N_b and the average value of N_{Tx} determined using the optimum thresholds, are shown in Fig. 2. One important feature of Fig. 2 is that N_{Tx} is independent of N_b for small values of N_b. The other important feature is that N_{Tx} is proportional to the square root of N_b at high values of N_b[18]. Previously, these features have been used to predict that, when ISI is negligable, increasing the area of a SiPM by a factor *f* will reduce the irradiance needed to achieve a particular BER by a factor between $f^{1/2}$ and f [18]. Unfortunately, the results in Table 1 show that increasing the area of a SiPM also increases the width of the output pulses. This strategy may therefore only be succesful at lower data rates.

In the past optical filters have been used to reduce the impact of ambient light. However, these filters won't protect the SiPM from one non-ideal characteristic of some transmitters. In particular transmitters need a wide bandwidth to support data rates of several Gbps and wide bandwidths are achieved by not turned off transmitters when they are transmitting a zero. The ratio between the transmitters output powers when transmitting a zero, P_0, and when transmitting a one, P_1, is characterised by the extintion ratio (EXR),

$$EXR = P_1/P_0 \tag{3}$$

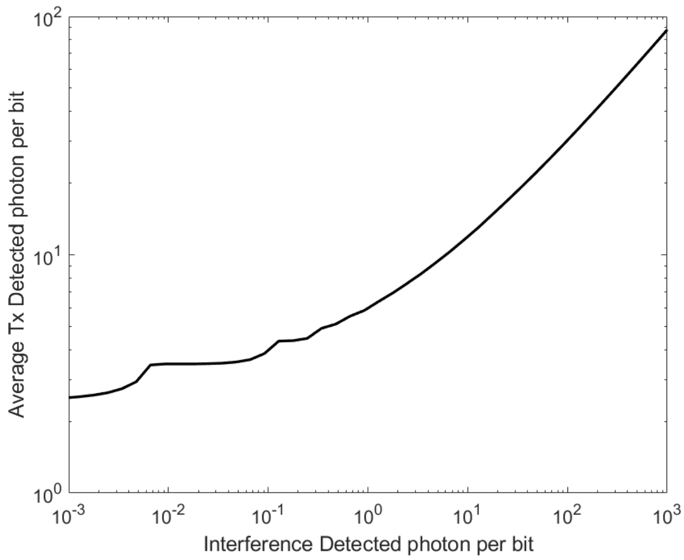

Figure 2 The average number of additional detected photons per bit required to achieve a BER of 3.8 × 10-3 when varying numbers of photons per bit are detected when a zero is being received.

The results in Fig. 3 show that the extinction ratio can have a significant impact on the number of photons per bit needed to achieve a particular BER. Previously, the extinction ratio of a L405P20 405 nm laser diode used to transmit OOK data rates of less than 2.4 Gbps, was found to be 15. The impact of this extinction ratio had to be taken into account when predicting the performance a system accurately [18]. However, at lower extintion ratios, for example those less than 5, the number of photons per bit increases very rapidly as the EXR reduces. The EXR of the transmitter could therefore play a key role in determining the performance of a system.

3.2 Impact of non-linearity on BER

The count rate for a SiPM such as the J30020 can be related to the irradiance of monochromatic light falling on the SiPM, L, by [4]

$$\mathbf{C_{rate}} = \boldsymbol{N_{cells}\alpha L/(1+\alpha\tau_p L)} \tag{4}$$

where N_{cells} is the number of microcells in the SiPM and τ_p is a characteristic time. In addition the parameter α is

$$\alpha = \eta(V_{ov},\lambda)A_{\mu}/E_p \tag{5}$$

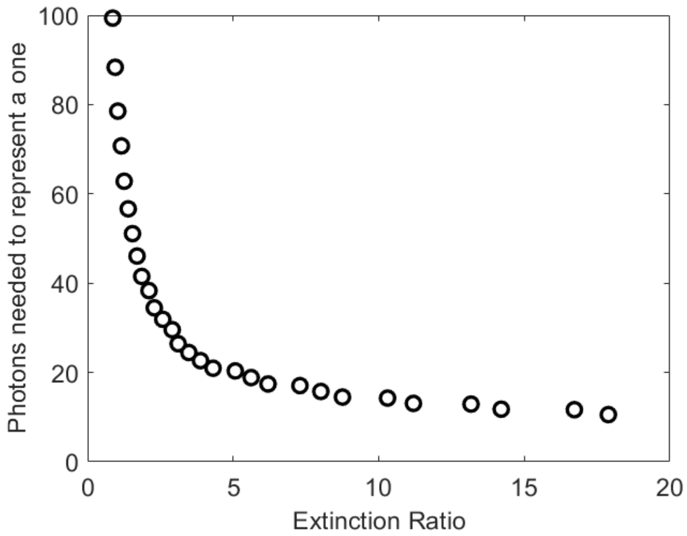

Figure 3 The impact of the extinction ratio of the transmitter on the number photons per bit needed to represent a one and achieve a BER of 3.8×10^{-3}.

where $\eta(V_{ov}, \lambda)$ is the PDE of the SiPM at a particular over-voltage, V_{ov}, and wavelength, E_p is the energy of photon at this wavelength and A_μ is the active area of a microcell.

Equation (4) was derived assuming that a microcell can't detect photons for a time, known as the dead-time, whilst it recovers after detecting a photon [4]. This equation has previously been used to explain the relationship between the current needed to sustain the SiPM bias voltage and the monochromatic irradiance falling on the SiPM [11]. However, recent simulations showed that the assumption that a microcell can't detect a photon during its dead-time isn't correct [19]. Fortunately, if τ_p is approximately 2.2 times the recovery time listed in the datasheets and Table 1, (4) can be used to explain the current needed to sustain the SiPM bias voltage. In addition, it has been shown that this non-linear response occurs on the fast output used to create a receiver [19].

Previously, the SiPM's non-linear response occurred because the SiPM was exposed to ambient light [19]. However, it will also occur at high transmitter irradiances. An important difference between ambient light and light from the transmitter is that the light from the transmitter is modulated. For a J30020 SiPM, at OOK data rates of 1 Gbps or higher τ_p is greater than 33 times the bit time. Under these conditions the varying irradiance from the transmitter is expected to be indistinguishable from a constant ambient irradiance. It is therefore expected that the non-linearity observed at high ambient light irradiances will also be observed at higher OOK data rates. If this is the case then the irradiance, L_{NL}, needed to achieve a particular count rate, C_{rate}, can be calculated by rearranging (4) to give

$$\boldsymbol{L_{NL}} = \boldsymbol{C_{rate}} / (\boldsymbol{\alpha}(\boldsymbol{N_{cells}} - \boldsymbol{\tau_p} \boldsymbol{C_{rate}})) \quad (6)$$

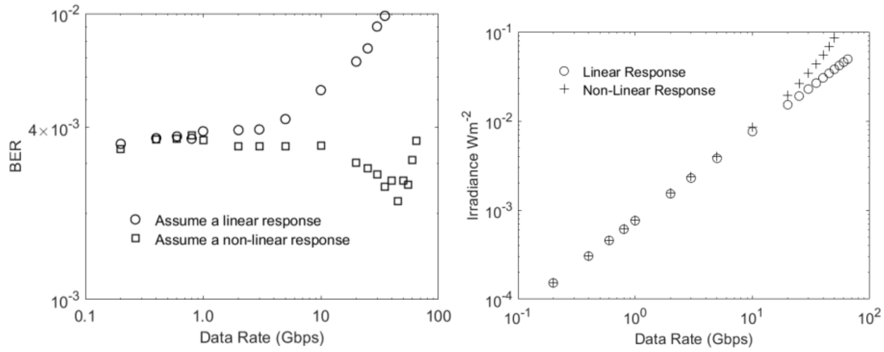

(a) (b)

Figures 4 (a) The BER from a simulation which assumed a fast output pulse width of zero and when a zero is transmitted there are no detected photons. This means that to achieve the target BER of 3.8×10^{-3} approximately 5.2 photons have to be detected. (b) The irradiances used to generate the results in Figure 4 (a).

The usefulness of (6) has been investigated using Monte-Carlo simulations. In these simulations the BER achieved at different data rates when the SiPM is assumed to have a linear response were first calculated. Then the BER was calculated when (6) was used to compensate for a non-linearity. The results in Fig. 4 (a) show the simulated BER for a J30020 SiPM with an output pulse width of zero. These results show that if the SiPM is assumed to have a linear response then the target BER is only achieved for data rates less than 1 Gbps. In contrast, using (6) to determine the irradiance needed to achieve the required count rate maintains the BER to less than the target BER up to 100 Gbps. The deviations in BER from the target value arise because (6) isn't a perfect representation of the non-linearity and the results in Fig. 1 show that the BER is very sensitive to the number of detected photons per bit. Taking these factors into consideration the results in Fig. 4 (a) confirm that the same non-linearity occurs when high count rates arise from either ambient light or high data rates.

The irradiances used to obtain the results in Fig. 4 (a) are shown in Fig. 4 (b). These results show that the non-linearity has very little effect for irradiances less than the maximum irradiance that would be available from a 405 nm transmitter in a typical office [12]. Furthermore, these results indicate the possible impact of the finite width of the fast

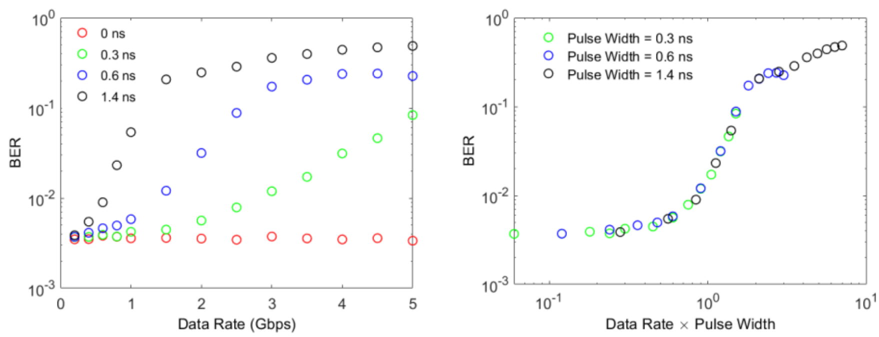

(a) (b)

Figures 5 The BER achieved when 5.2 photons are detected per bit when a one is transmitted. (a) shows the results at different data rates compared to the ideal result. (b) shows that the important parameter is the product of the pulse width and the data rate.

output pulses. In particular, in previous experiments with a J30020 a data rate of 3 Gbps was achieved at a irradiance of approximately 100 mWm^{-2} [11]. In contrast, the results in Fig. 4 (b) show that if the width of the fast output pulses is zero a data rate of 50 Gbps could be achieved at this irradiance. These simulation results show that the SiPMs non-linearity isn't the factor that has previously limited the data rates that have been achieved.

3.3 Impact of pulse width

The impact of the finite width of fast output pulses has been investigated by determining the BER at various OOK data rates. In these simulations the non-linearity was taken into account by using (6) to determine the transmitter irradiance which will generate 5.2 additional photons per bit when a one is transmitted. The results for a pulse width of 1.4 ns were included in these simulations to represent a J30020. The results for this pulse width in Fig. 5 (a) show that the pulse width has an impact of the BER at data rates of less than 1 Gbps. In particular, when the pulse width is 1.4 ns the BER is 10^{-2} at approximately 600 Mbps. However, the results in Fig 4 (a) show that the non-linearity doesn't cause the same BER until approximately 35 Gbps. This confirms that the pulse width has a significant impact on the performance of the J30020.

The impact of the ISI caused by the width of the output pulses is expected to depend upon the ratio of the pulse width to the bit time. Since the OOK data rate is inversely proportional to the bit time this is the same as the product of the data rate and the output pulse width. The results in Fig. 5 (b) confirm that the impact of ISI depends upon the ratio between the pulse width and the bit time. Furthermore, the results in Fig. 5 (b) show that the BER only starts to increase rapidly when the pulse width equals the bit time. This means that halfing the width of the fast output pulses will double the data rate at which ISI creates a significant power penalty.

3.4 The pulse width penalty

The penalty from ISI alone has been determined by simulating a SiPM with the same parameters as a J30020, except that the recovery time was set to 1 ps. This recovery time is significantly shorter than the minimum timestep of the simulations. Consequently, all microcells fully charged at each simulated timestep and the SiPMs response is therefore linear. For each simulation the data rate was set. Then the BER after DFE was evaluated for count rates that achieved BERs between 10^{-3} and 10^{-2}. Linear interpolation and this data

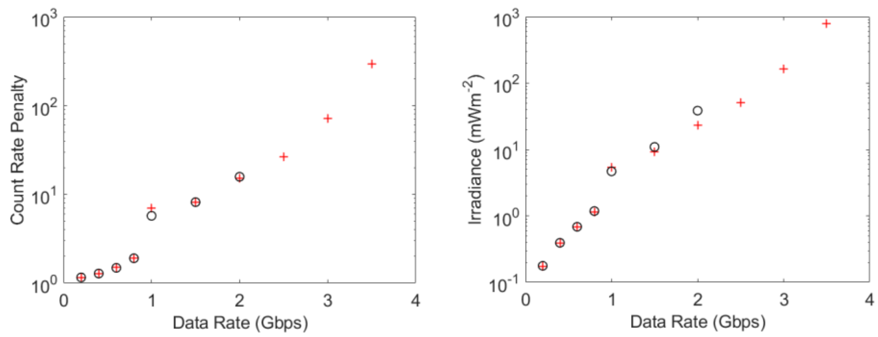

(a) (b)

Figures 6 (a) The count rate penalty required to achieve a BER of 3.8 ×10^{-3} at data rates that are high enough for the fast output pulses to create ISI. The parameters for a J30020 were used to obtain the simulation results shown in black circles (o). The simulation results shown as red crossed (+) were obtained assuming that the J30020 SiPM had a recharge time of 1 ps, and therefore has a linear response. The irradiance needed by a J30020 to support these count rate penalties are shown in (b).

was then used to estimate the count rate that would give a BER of 3.8×10^{-3}. These results were then expressed as a count rate penalty, which is the count rate needed to achieve a BER of 3.8×10^{-3} divided by 5.2 times the data rate, which is the count rate that is expected to achieve this BER. To include the effect of the SiPMs non-linearity this process was then repeated for an SiPM with the same recovery time as the J30020.

The results in Fig. 8 (a) show that for data rates less than 2 Gbps, the non-linearity has no impact on the count rate penalty. However, the results in Fig 8 (b) show that the non-linearity increases the irradiance required to obtain the same count rate at 2 Gbps. Furthermore, by 2 Gbps the count rate penalty is approximately 16. This means that the required number of photons per bit when a one is transmitted has increased from 6 at 200 Mbps to 82 at 2 Gbps.

Some results for the SiPM with the same parameters as a J30020 are missing from Fig. 6 because it wasn't possible to achieve a BER of 3.8×10^{-3} at the higher data rates. The results in Fig. 7 shows that at 2.5 Gbps the BER starts to increase as the count rate increases. This creates a minimum BER above the required BER. A minimum BER as the irradiance, and hence count rate, increases has been observed experimentally previously [10]. This previously unexpected behaviour was found to be due to a new form of ISI caused by the SiPMs non-linearity. A comparison between the count rates of these simulations and the maximum count rate of the simulated SiPM suggests that this phenomenon has become important once the count rate is 40% of the maximum count rate.

3.5 Improving the agreement between experimental and simulated results

Using the parameters of the J30020 created the opportunity to compare the simulation results with experimental results. The possible negative impacts of the transmitters bandwidth and/or extinction ratio would explain simulation results that were better than the experimental results. However, the results in Fig. 8 (b) predict that higher irradiances are required than observed experimentally, e.g. the experimental results gave a data rate of approximately 3 Gbps at 100 mWm^{-2}, whilst the simulation results suggests that this

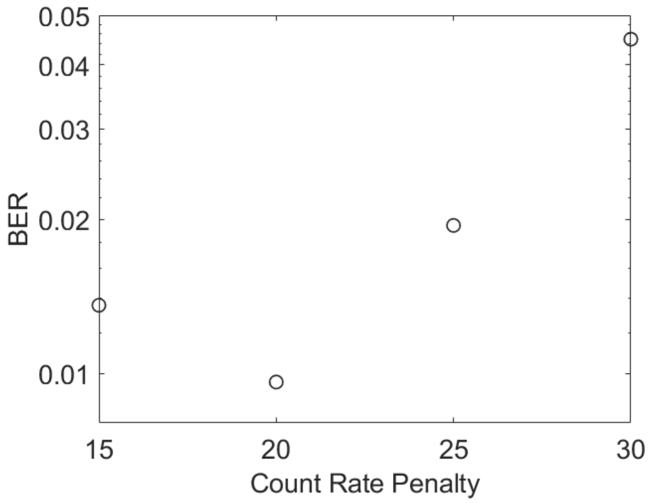

Figure 7 The simulated BER of a SiPM with the same parameters as a J30020 at 2.5 Gbps.

data rate is impossible. This suggests that the 1.4 ns Guassian pulses used in the simulator are pessimistic. Reducing the fast output pulse width by a factor of 1.5 means that the simulation predicts a data rate of 3 Gbps at an irradiance of 97 mWm^{-2}. It appears that reducing the pulse width in the simulator by a factor of 1.5 improves the accuracy of the simulation results.

4. Discussion

4.1 Previous Published Work

Previously, the performance of receivers containing J30020 and J30035 have been compared [11]. These two SiPMs have very similar output pulse widths. However, its larger number of microcells and faster recovery time means that the maximum count rate of the J30020 is four times the maximum count rate of the J30035. This significant difference was the motivation for a previous comparison of receivers containing these two SiPMs [11]. This comparison showed that at an irradiance of 100 mWm^{-2} changing the SiPM increased the data rate from 2.4 Gbps to 3.0 Gbps. This small increase relative to the increase in maximum count rate can now be seen to arise from the rapidly increasing count rate penalty at high data rates.

4.2 Selecting between available SiPMs at 405 nm

The results in Fig 4 (a) show that the non-linearity alone begins to impact the achieved BER at 1 Gbps. This corresponds to an average count rate 26 Gcps, which is approximately 5% of the maximum count rate. This strict definition of the end of the linear regions arises from the sensitivity of the BER to the number of detected photons per bit shown in Fig. 1. However, the sensitivity of BER to the detected photons per bit means that the power penalty for higher count rates will be relatively small. This strict definition of the end of the linear regime therefore simply highlights when the transmitter irradiance may need to be increased slightly to achieve the required BER.

The simulation results suggest two more important criteria that should be considered when selecting an existing SiPM for incorporation into a receiver. These are:

(i) The results in Fig. 6 (a) show that the effects of the non-linearity and the pulse-width are independent if the count rate is less than 40% of the maximum count rate. Even when the pulse-width penalty is negligible the non-linearity would almost double the irradiance required to achieve a particular BER. It may therefore be prudent to expect a SiPM to operate with count rates less than 40% of its maximum count rate.

(ii) The results in Fig. 6 (a) also show that the count rate power penalty is less than 2 if the bit time is less than the pulse width. To avoid a significant increase in required irradiance the transmitted data rate should ideally be less than the data rate whose bit time equals the pulse width.

The results that arise from applying these two conditions, Table 2, shows that if they are applied the suggested data rates for the J30020 is less than the maximum data rate that has been reported [11]. This is because, like the C10010 and the C30020, the data rate at which condition (i) is reached for the J30020 is much higher than that required for ISI to double the required irradiance, condition (ii). This means that these SiPMs have the capacity to tolerate an ISI power penalty significantly larger than 2.

Table 2. Two important parameters of the onsemi SiPMs together with the data rates determined by the two criteria described in the text.

Name	Maximum Count Rate (Gcps)	Fast Output Pulse Width from the data sheet (ns)	Estimated Equivalent Gaussian Fast Output Pulse Width (ns)	Data Rate (i) (Gbps)	Data Rate (ii) (Gbps)
RB10010	162.7	2.3	1.5	12.5	0.7
RB 10020	34.4	2.0	1.3	2.6	0.8
RB 10035	3.9	3.7	2.5	0.3	0.4
C10010	261.8	0.6	0.4	20.1	2.5
C10020	25.6	0.6	0.4	2.0	2.5
C10035	2.8	0.6	0.4	0.2	2.5
C30020	217.4	1.5	1.0	16.7	1.0
C30035	26.5	1.5	1.0	2.0	1.0
C30050	7.6	1.5	1.0	0.6	1.0
C60035	90.8	3.2	2.1	7.0	0.5
J30020	436.7	1.4	0.9	33.6	1.1
J30035	57.3	1.5	1.0	4.4	1.0
J40035	87.7	1.7	1.1	6.7	0.9
J60035	202.7	3.0	2.0	15.6	0.5

The J30020 has more microcells, a higher PDE and a higher maximum count rate than the C30020. The estimated performance of a J30020 and a C10010 are therefore shown in Fig. 8. As expected the results in Fig. 8 show that there large maximum count rates allow these two SIPMs to operate at data rates at which they incur a significant ISI power penalty. However, it is also clear that despite having faster output pulses the smaller area of the C10010 means that it is only expected to perform better that the J30020 at data rates higher than 3 Gbps. At these data rates the performance of the J30020 is limited by a combination of ISI power penalty and saturation of its non-linear response. However, its smaller area means that the C10010 is only a better choice than the J30020 at irradiances that are not eye-safe [12].

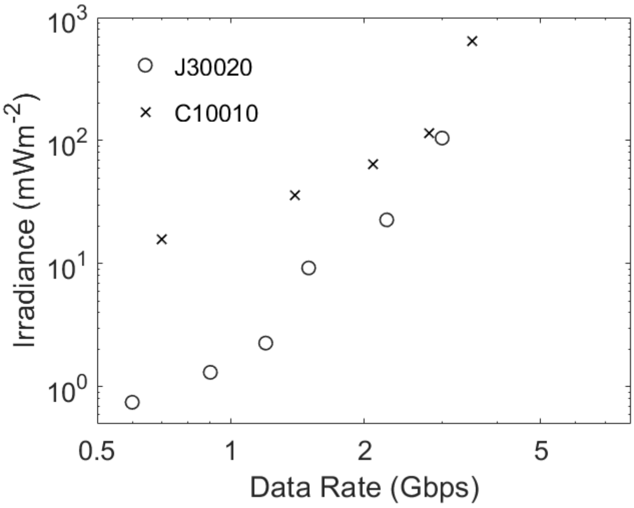

Figure 8 The estimated performance of a J 30020, a C1000 and a C10020. These results were obtained by first using the ratio of the bit time to the estimated equivalent Gaussian pulse width to determine the ISI count rate penalty using the results in Fig 7 (a). This was then converted to the required irradiance using the relevant SiPM parameters and equation (6).

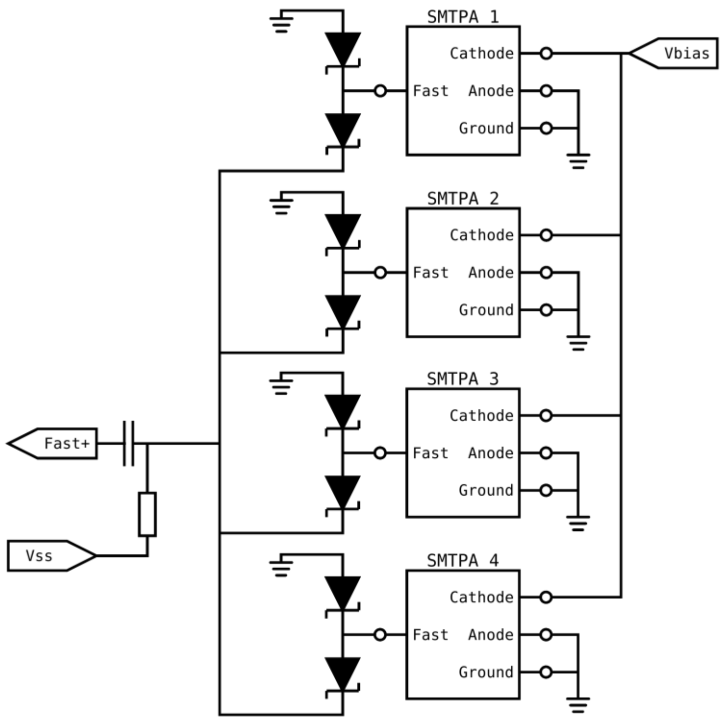

Figure 9 Schematic showing a method of combining multiple SiPM fast outputs together using diode pairs [27].

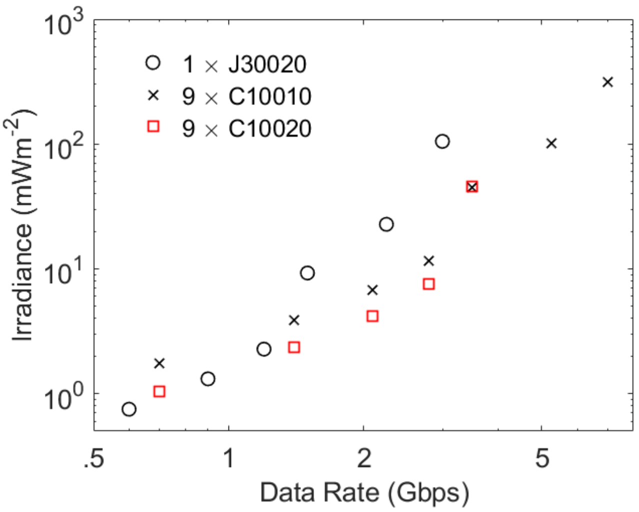

Figure 10 The potential performance of a J 30020 and combinations of 9 C10010 SiPMs and 9 C10020 SiPMs. These results were obtained using the same methodology as used to obtained the results in Fig 9.

4.2 Using Diodes to add SiPMs

Operating at OOK data rates whose bit time is significantly shorter than the duration of the SiPM's output pulses incurs a significant power penalty. This suggests that the primary characteristic to consider when selecting a SiPMs to use at higher data rates, e.g. OOK rates about 2 Gbps, should be the duration of the fast output pulses. Unfortunately, the results in Table 1 show that these SiPMs have a smaller area and therefore fewer microcells. The results in Fig. 8 show that this means that the J30020 is a better choice than the C10010 at eye safe irradiance. However, it is possible to use a pair of Schottky diodes on the fast output of each SiPM to add their fast output pulses without increasing the width of the output pulses [27]. Fig. 9 shows a schematic diagram of this idea, where Skyworks SMS7621 24 GHz schottky diode pairs are used to combine the outputs of the SiPMs. In this circuit the SiPMs are biased by connecting a bias voltage V_{bias}, to their cathode. The fast output of each SiPM is connected to the centre of a pair of schottky diodes, which are forward biased by the bias source V_{ss} so that each diode pair passes approximately 1 mA. An output pulse on one SiPM will cause the current through the associated diode pair to vary. This current then flows on a common line where it is added to the current flowing from other SiPMs. Any variation in this total current is converted to a voltage by the resistor connected to V_{ss}. The high frequency content of this voltage passes through a capacitor to Fast+ which is the shared output from all the SiPMs.

The potential advantages of using more SiPMs with narrow fast output pulses has been investigated by assuming that it is possible to increase the number of microcells in a C10010 and C10020 without changing any of the other parameters. The results in Fig. 10 confirm that increasing the effective area of the SiPM reduces the irradiance required to support a particular data rate. The results for the combination of 9 C10020 SiPMs show that they might be the best choice for data rates up to approximately 3 Gbps. However, there significantly lower maximum count rate then causes a rapid increase in the required irradiance at approximately the data rates in Table 2. In contract, their large maximum count rates mean that both the J30020 and the combination of 9 C10010 SiPMs can operate a data rates well above those in Table 2. The difference now is that the increase in area means that the combination of C10010 SiPMs is a better choice at data rates of approximately 1.5 Gbps,

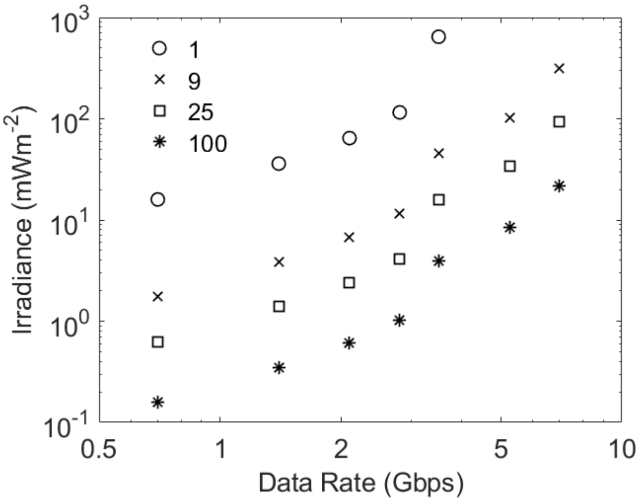

Figure 11 The potential performance of varying numbers of C10010 SiPMs working in parallel. These results were obtained using the same methodology as used to obtained the results in Fig 9.

which is close to the data rate at which ISI caused by the fast output pulses is expected to impact the performance of the J30020.

The possible benefits of using even more SiPMs in parallel is shown in Fig. 11. This figure confirms that adding more SiPMs in parallel will reduce the irradiance required to support a particular data rate. The ideal conditions assumed in these estimates, for example the absence of ambient light and an infinite extinction ratio on the transmitter, mean that the same number of photons per bit have to be detected. This means that at low data rates the required irradiance is inversely proportional to the number of SiPMs. However, the important comparison is the data rate that can be supported at a particular irradiance. At irradiances of approximately 4 mWm^{-2} an array of 25 C10010 SiPMs is expected to support 2.8 Gbps, whilst the array of 100 C10010 SiPMs would support 3.5 Gbps. These results show that the rapid rise in the count rate penalty at high data rates limits the performance improvements that can be achieved by increasing the number of SiPMs acting in parallel.

4.3 Exploiting the existing parallel fast outputs

A problem with using multiple SiPMs is that their price isn't proportional to their area. Consequently, an array of SiPMs would cost significantly more than a single SiPM with the same area. An alternative way of reducing the width of fast output pulses is suggested by a close inspection of the back side of the larger SiPMs produced by onsemi. This inspection shows that these SiPMs have multiple fast outputs which are connected together to create one fast output [24]. In particular, TSVs are used at several locations on the SiPM to connect fast outputs for different areas of the SiPM to its bottom side. These fast outputs are then connected together by metal traces. The resulting combined fast output is then connected to a single output pad. Fig. 12 (a) shows that a 3 mm by 3 mm J series SiPM, has six fast outputs which are connected together to a single pad [28]. Using a connection for each of these areas would create an array of 6 SiPMs with an area of 1.5 mm^2 each. These six outputs could be made available separately by a relatively small change at the end of the manufacturing process. They could then be combined using the method in Fig. 9. The result would be a 9 mm^2 SiPM with a fast output width of less than 1 ns.

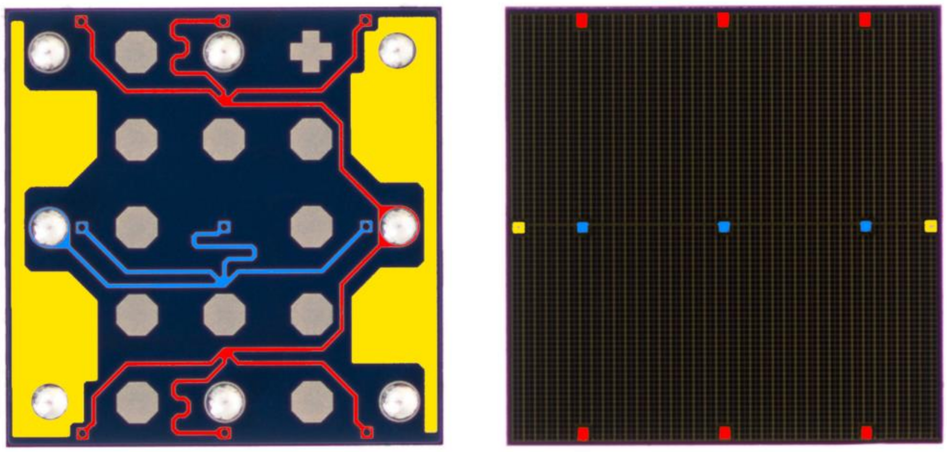

(a) (b)

Figure 12 A view of the J-Series 30035 SiPM, (a) shows the back of the SiPM where different traces are highlighted different colors for visibility. Yellow is the cathode (connected to bias source), blue is the anode (connected to ground, or a series resistor to measure instantanous bias current). Red traces are the fast outputs. The fast output on this device is combined from six separate regions. (b) shows the top of the SiPM, where the through silicon vias connect to the traces on the rear. (Adapted From [28])

4.4 Selecting between SiPMs for NIR

Experiments have been performed with 405 nm light to limit the impact of ambient light from white LEDs. However, this choice of wavelength limited the eye-safe power limit [12].

Table 3 Key parameters for the two series of commercially available SiPMs manufactured by onsemi including their PDE at 850 nm [22-24]

Name	Area (mm2)	Pitch (µm)	Number of µcells	Recovery Time (ns)	Maximum Count Rate (Gcps)	PDE at 850nm	Fast Output Pulse Width (ns)
RB10010	1	10	4296	12	162.7	0.07	2.3
RB10020	1	20	1590	21	34.4	0.12	2
RB10035	1	35	620	73	3.9	0.17	3.7
J30020	9	20	14410	15	436.7	0.025	1.4
J30035	9	35	5676	45	57.3	0.03	1.5
J40035	16	35	9260	48	87.7	0.03	1.7
J60035	36	35	22292	50	202.7	0.03	3

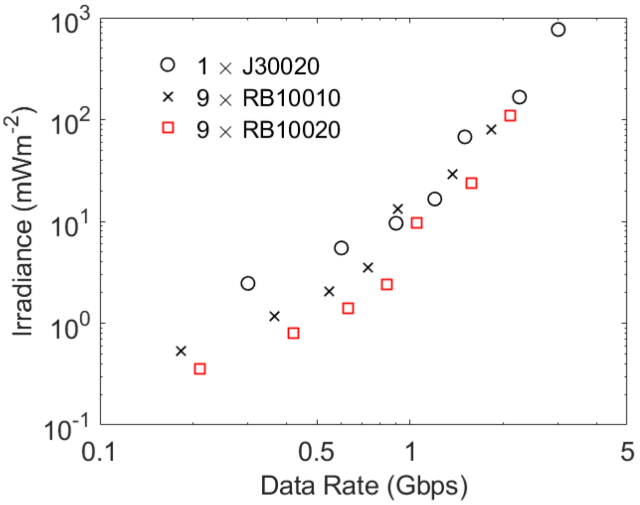

Figure 13 The potential performance of a J 30020 and combinations of 9 RB10010 SiPMs and 9 RB10020 SiPMs. These results were obtained using the same methodology as used to obtained the results in Fig 8.

Changing to 850 nm would increase the eye-safe power limit by a factor of approximately 50 and mean that existing high bandwidth 850 nm transmitters could be used.

The RB series of SiPMs have a higher PDE at 850 nm than the J series SiPMs. This would suggest that they are the better choice for operation with 850 nm transmitters. However, as shown in Table 3, they also have broader fast output pulses. The potential performance of a J30020 and arrays of 9 RB10010 SiPMs and 9 RB10020 SiPMs are shown in Fig. 13. All these systems have the same overall area. Consequently, their higher PDE means that the two systems made from RB series SiPMs support the lower data rates at lower irradiances than the J30020. However, at data rates of more than 1 Gbps the narrower output pulses of the J30020 means that the performance of this SiPM is expected to be similar to the performance of the array of RB series SiPMs. Cost would then favour the J30020.

At 405 nm an eye-safe transmitter in a typical office would deliver 3 mWm^{-2} at the edge of its coverage area [12]. Changing to 850 nm would increase this to approximately 150 mWm^{-2}. The results in Fig. 13 suggest that at this irradiance the SiPMs would support approximately 2 Gbps. This is a little higher than the data rate, 1.4 Gbps, achieved using 405 nm transmitter in the same scenario. However, the results with a 405 nm transmitter was obtained in 500 lux of ambient light using filters to protect the SiPM from ambient light. Despite the increase in eye-safe power a change to 850 nm is therefore not expected to support significantly higher data rates.

4.5 Designing application specific SiPMs

The results show that any new application specific integrated circuit (ASIC) designed to act as a receiver should have significantly faster output pulses than existing SiPMs. This emphasis suggests that the microcells in the ASIC might have a digital output. SiPMs with digital outputs have been integrated into receivers previously [29, 30]. However, both the SiPMs used in these experiments were created on one chip. This meant that the digital logic circuits alongside each SPAD reduced the overall fill-factor, and hence PDE, of the SiPM.

Fortunately, since these SiPMs were manufactured the ability to stack two chips has been developed [31]. If one of these chips is used to create an array of APDs and the other to create a matching array of ancillary circuits then this technology avoids the trade-off between circuit complexity and fill-factor. In addition, this technology means that the two chips can be made using the manufacturing processes best suited to their function. These advantages mean that stacked systems, often known as SPAD arrays, have been created in which one of these chips contains an array of APDs and the other chip contains a matching array of quenching circuits and relatively sophisticated digital circuits [31].

The existing stacked SPAD arrays have been designed for applications such as LIDAR and low-light imaging. However, they contain components that could be used to create a receiver. The most important component which could be used in a receiver is the APDs in the first chip. These have been made using a variety of manufacturing processes and some include additional features that increase the PDE at some or all wavelengths. One feature used in some devices is a charge-focusing SPAD, in which the electric field in the APD guides photon-generated electrons into a central avalanche region [32]. This approach results in a fill-factor of 100% and a PDE of approximately 40% at 405 nm. Furthermore, SPADs can be created with a 6.39 μm pitch and in arrays of 2,072 by 1,548 [32].

A key function of the ancillary circuits in the second chip is to quench the otherwise self-sustaining avalanche processes. In order to reduce after-pulsing this can be done by combining a passive quenching process with an active reset (a combination known as PQAR). To achieve this a MOSFET is connected in series with the APD to create a load which reduces the bias voltage across the APD when an avalanche occurs. The resulting change in the voltage across the APD is then detected by a digital circuit. This circuit is designed to hold the APD bias voltage below the breakdown voltage for a controlled time. During this time any charge trapped in the APD can escape without creating an after-pulse. However, the cost of suppressing after-pulses is that the SPAD can't detect a photon and so this time is the dead time for the SPAD. At the end of the dead time the digital circuits rapidly resets the APD bias voltage. Since this minimizes the probability that a photon is detected whilst a SPAD is being recharged it reduces the risk that the SPAD can be paralysed at high irradiances [33]. Depending upon the application the digital signal generated by an avalanche event can be processed in one of several different ways. An example of the circuit complexity that can be achieved is a low light image sensor [34]. In this case the ancillary circuit associated with each SPAD included a quenching circuit, and a 9-bit counter to count the detected photons. However, this might overflow and so it also contained an additional 5 bit latch which, together with the 9-bit latch from the counter, can store a 14-bit code that represents the time at which the counter overflows. It also includes a 15 bit multiplexer to connect the contents of these 14 latches and an overflow flag to a shared 15 bit bus. All of this functionality was achieved in a 12.24 μm pitch.

This example system indicated the functionality that can be achieved in an area which is smaller than the area of the microcells in most existing SiPMs. However, the challenge when supporting multi-Gbps OOK data rates is that data has to be obtained from each array element in a small fraction of a nanosecond. Fortunately, the location at which a photon is detected isn't important. This means that each SPAD can be allowed to transmit its response to a detected photon as soon as it occurs. Furthermore, the method of combining the SPAD outputs should support the simultaneous detection of a few photons and different modulation schemes.

Table 4 Comparison between a J30020 and a potential stacked SPAD receiver.

Name	J30020	Stacked
Area (mm2)	9	9
Pitch (μm)	20	12.24
Number of μcells	14410	60073
Recovery Time/Dead Time (ns)	15	8
Maximum Count Rate (Gcps)	436.7	7509
PDE at 405nm	0.38	0.4
Fill Factor	0.62	1
Fast Output Pulse Width (ns)	1.4	0.1

One way to accommodate simultaneous detection of photons would be to generate a narrow output current pulse when an avalanche occurs. In the exemplar system, the quenching and digital logic circuits were manufactured in a 40 nm CMOS process [34]. A 1 μm wide transistor manufactured in a 40 nm process can pass a current of approximately 400 μA [35]. In addition, the maximum frequency at which these transistors can amplify a signal is at least 200 GHz [35]. This suggests that it should be possible to generate 10 ps current pulses when a photon is detected. Furthermore, it should be possible to create trans-impedance amplifiers on the same chip which create an analogue output voltage that is proportional to sum of these short current pulses.

Table 4 contains a comparison between a J30020 and a possible stacked SPAD receiver. The two systems are assumed to have the same area. The pitch of the stacked receiver is assumed to be the same as the pitch of the exemplar system [34]. The result is a four-fold increase in the number of microcells. In addition, it is assumed that the dead time of the stacked system is 8 ns. This is the time previously used to suppress after-pulsing [36]. Finally, although it may be possible to create 10 ps output pulses, a conservative estimate of 100 ps, is included in the table.

If the assumed fast output pulse width can be achieved then the stacked system would not suffer from ISI caused by the receiver for data rate less than 10 Gbps. At lower data rates it would therefore require an average of approximately 2.6 photons per bit to achieve a BER of 3.8×10^{-3}. A data rate of 10 Gbps would then be achieved when the average irradiance from a 405 nm transmitter is 1.8 mWm^{-2}. This is less than the irradiance that can be obtained from an eye-safe 405 nm transmitter in typical office [12]. This receiver therefore has the potential to deliver data rates of up to 10 Gbps in a typical office.

A potential hurdle to achieving 10 Gbps using 405 nm is the bandwidth of 405 nm transmitters. In this case it may be prudent to change to 850 nm transmitters designed to deliver data rates of more than 10 Gbps. At 850 nm the SPAD could have a PDE of 30% or more [32]. In this case, the lower energy of 850 nm photons, means that 10 Gbps could be achieved at an irradiance of 1.1 mWm^{-2}. This would be eye-safe and could be delivered using an 850 nm transmitter that is designed to deliver 10 Gbps or higher [37]. Two or more of these devices could be used separately or in parallel to cover the 2 m by 2 m area covered by a single transmitter in the typical office environment [12]. The result would be an irradiance that could support 10 Gbps.

In the absence of an ISI power penalty from either the transmitter or the receiver 10 Gbps requires an average count rate of approximately 26 Gcps, which is a tiny fraction of the potential maximum count rate of 7509 Gcps. This maximum count rate suggests that the stacked receiver would have the capacity to tolerate a count rate penalty of 144. However, to avoid the negative impact from the non-linearity it may be more efficient to limit the penalty to half this value. This would suggest that the receiver could support data rates of 30 Gbps. This is slightly higher than the data rate that is supported by receivers designed for fiber optical communications [37]. However, the existing receivers need 0.3 mW of received optical power to support a data rate of

25.78 Gbps and a BER of 5×10^{-5}. Under ideal conditions this BER requires an average of approximately 5 photons per bit. However, the extinction ratio of the transmitter in this system is 2 and Fig. 3 shows that this means that the average number of photons per bit must be approximately 60. Taking these factors into account, without any ISI penalty the stacked receiver would require only 0.6 µW at the same data rate, wavelength, BER and extinction ratio. Even with a significant ISI penalty the stacked receiver would therefore be expected to require only a small fraction of the optical power of the existing receiver to support 25.78 Gbps.

Furthermore, the stacked receiver's dead-time in Table 4, 8 ns, is the dead time used to reduce the after-pulsing probability for applications were after-pulses maybe a significant problem. In contrast, previous Monte-Carlo simulations have replicated experimental results despite the fact that after-pulsing isn't included in these simulations. This suggests that it may be possible to reduce the dead time of these systems significantly. The result could be a receiver that can support data rates approaching 1 Tbps.

5. Conclusions

Results that have been reported which confirm that SiPMs with narrow output pulses should be preferred when selecting SiPMs for incorporation into VLC or OWC receivers. Furthermore, the irradiance required to achieve a particular BER increases rapidly once the bit time is shorter than the output pulse width.

Although the pulse width is a very important parameter the SiPM non-linearity must be taken into account. In particular, it is suggested that a SiPM should operate with a count rate less than 40% of its maximum count rate.

The need to detect a constant number of photons per bit means that increasing the area of a SiPM should reduce the irradiance needed to support a particular data rate. Unfortunately, increasing the area of a single SiPM of a particular type increases its pulse width. The trade-off between area and pulse width can be avoided by using diodes to add the outputs of SiPMs acting in parallel. However, using this method to significantly increase the data rate would be expensive. This cost increase could be reduced by using a small change in the last stages of the manufacturing process of individual larger SiPMs to create single SIPMs with multiple outputs that have narrower output pulses.

Reasons for a change of transmitter wavelength from 405 nm to 850 nm have been highlighted. However, results have been presented which suggest that the benefits of this change will be relatively small.

Finally, a brief survey of systems made by stacking arrays of SPADs onto a second chip has been presented. This survey suggests that this new technology could dramatically improve the performance of receivers. The result would be a receiver that is significantly better than existing receivers for fibre-optic communications operating at 25.78 Gbps. Factors that would make it possible to create receivers operating at significantly higher data rates have been highlighted.

Author Contributions: "Conceptualization, W.M. and S.C.; methodology, S.C.; software, W.M.; validation, S.C. and W.M.; data curation, S.C.; writing—original draft preparation, S.C.; writing—review and editing, W.M and S.C.; supervision, S.C.; All authors have read and agreed to the published version of the manuscript."

Funding: This research has been supported by the UK Engineering and Physical Sciences Research Council (EPSRC) under Grant EP/R00689X/1. In addition W. Matthews would like to thank the EPSRC for the grant to support his DPhil.

Data Availability Statement: The data presented in this study, and the accepted version of this paper, are openly available in the Oxford Research Archive (ORA), https://doi.org/10.5287/bodleian:ORodKRbm0

Conflicts of Interest: "The authors declare no conflict of interest."

References

1. Haas H., Elmirghani J. and White I., "Optical Wireless Communication" Phil. Trans. R. Soc. A, 2020 vol. 378.
2. Khalighi M., Hamza T., Bourennane S. , Léon P. and Opderbecke J. , "Underwater Wireless Optical Communications Using Silicon Photo-Multipliers", IEEE Photonics Journal, **2017**, vol. 9, no. 4, pp. 1-10.
3. Leon, P., Roland, F., Brignone, L., Opderbecke, J., Greer, J., Khalighi, M.A., Hamza, T., Bourennane, S. and Bigand, M., "A new underwater optical modem based on highly sensitive Silicon Photomultipliers," OCEANS 2017, Aberdeen, UK 19-22 June 2017.
4. Zhang L.,Chitnis D.,Chun H. , Rajbhandari S., Faulkner G., O'Brien D., and Collins S., "A comparison of APD- and SPAD-based receivers for visible light communications", J. Lightw. Technol., **2018**, vol. 36, no. 12, pp. 2435–2442.
5. Ahmed Z. , Zhang L. , Faulkner G. , O'Brien D. and Collins S., "A Shot-Noise Limited 420 Mbps Visible Light Communication System using Commercial Off-the-Shelf Silicon Photomultiplier (SiPM)," 2019 IEEE International Conference on Communications Workshops (ICC Workshops), Shanghai, China, 20-24 May 2019.
6. Ahmed Z. , R. Singh R. , Ali W. , Faulkner G. , O'Brien D. and Collins S., "A SiPM-Based VLC Receiver for Gigabit Communication Using OOK Modulation", IEEE Photonics Technology Letters, **2020**, vol. 32, no. 6, pp. 317-320.
7. Zhang L., Tang X., Sun C., Chen Z., Li Z., Wang H., Jiang R., Shi W., and Zhang A., "Over 10 attenuation length gigabits per second underwater wireless optical communication using a silicon photomultiplier (SiPM) based receiver,'' Opt. Exp., **2020**, vol. 28, no. 17, p. 24968.
8. Khalighi M.A. , Akhouayri H. and Hranilovic S., "Silicon-Photomultiplier-Based Underwater Wireless Optical Communication Using Pulse-Amplitude Modulation", IEEE Journal of Oceanic Engineering, **2020**, vol. 45, no. 4, pp. 1611-1621.
9. Tang, X., Zhang, L., Sun, C., Chen, Z., Wang, H., Jiang, R., Li, Z., Shi, W. and Zhang., A. "Underwater Wireless Optical Communication Based on DPSK Modulation and Silicon Photomultiplier," IEEE Access, **2020**, vol. 8, pp. 204676-204683.
10. Matthews W. , Ali W., Ahmed Z., Faulkner G. and Collins S., "Inter-Symbol Interference and Silicon Photomultiplier VLC Receivers in Ambient Light," in IEEE Photonics Technology Letters, **2021**, vol. 33, no. 9, pp. 449-452.
11. Matthews W., Ahmed Z., Ali W. and Collins S., "A 3.45 Gigabits/s SiPM-Based OOK VLC Receiver", IEEE Photonics Technology Letters, **2021**, vol. 33, no. 10, pp. 487-490.
12. Ali W., Faulkner G., Ahmed Z., Matthews W. and Collins S., "Giga-Bit Transmission between an Eye-Safe Transmitter and Wide Field-of-View SiPM Receiver", IEEE Access, **2021**, vol. 9, pp. 154225-154236.
13. Li Y., Hua Y., Henderson R.K. and Chitnis D., "A Photon Limited SiPM Based Receiver for Internet of Things," 2021 Asia Communications and Photonics Conference (ACP), Shanghai, China, 24-27 October 2021.
14. Zhang L., Jiang R., Tang X., Chen Z., Chen J. and Wang H., "A Simplified Post Equalizer for Mitigating the Nonlinear Distortion in SiPM Based OFDM-VLC System", IEEE Photonics Journal, **2022**, vol. 14, no. 1, pp. 1-7.
15. Huang S., Chen C., Bian R., Haas H., and Safari M., "5 Gbps optical wireless communication using commercial SPAD array receivers", Opt. Lett., **2022**, vol. 47, pp. 2294-2297.
16. Li, Y., and Chitnis, D. "A real-time SiPM based receiver for FSO communication.", SPIE Opto, San Francisco, California, United States, 3 March 2022.
17. Matthews W. and Collins S., "The negative impact of anode resistance on SiPMs as VLC receivers," 2022 17th PRIME Conference, Sardinia, Italy, 12-15 June 2022.
18. Ahmed Z., Ali W., Faulkner G. and Collins S., "A comparison of VLC receivers that incorporate two different SiPMs", **2022**, IEEE Photonics Journal, (submitted)
19. Matthews W, and Collins S. An Experimental and Numerical Study of the Impact of Ambient Light of SiPMs in VLC Receivers. MDPI Photonics, **2022**, Vol. 9, No. 12, p. 888.
20. Zhang L, Jiang R, Tang X, Chen Z, Li Z, Chen J. Performance Estimation and Selection Guideline of SiPM Chip within SiPM-Based OFDM-OWC System. MDPI Photonics, **2022**, Vol. 9, No. 9, p. 637.
21. He C, Lim Y. "Silicon Photomultiplier (SiPM) Selection and Parameter Analysis in Visible Light Communications." 2022 31st Wireless and Optical Communications Conference (WOCC) IEEE, Newark, USA , 11 August 2022
22. Hinrichs, M., Berenguer, P.W., Hilt, J., Hellwig, P., Schulz, D., Paraskevopoulos, A., Bober, K.L., Freund, R. and Jungnickel, V., A physical layer for low power optical wireless communications. IEEE Transactions on Green Communications and Networking, 2020, vol. 5 no. 1, pp.4-17.
23. https://www.onsemi.com/pdf/datasheet/microrb-series-d.pdf (Accessed on 20 June 2022).
24. https://www.onsemi.com/pdf/datasheet/microc-series-d.pdf (Accessed on 20 June 2022).
25. https://www.onsemi.com/pdf/datasheet/microj-series-d.pdf (Accessed on 20 June 2022).
26. https://www.onsemi.com/pub/Collateral/AND9770-D.PDF (Accessed on 20 June 2022).
27. https://www.onsemi.com/pub/Collateral/AND9772-D.PDF (Accessed on 20 June 2022).
28. https://uk.farnell.com/on-semiconductor/microfj-30020-tsv-tr1/sipm-ic-20um-odcsp-8/dp/2949096 (Accessed on 16 December 2022)
29. E. Fisher, I. Underwood, and R. Henderson. "A reconfigurable single-photon-counting integrating receiver for optical communications." IEEE Journal of Solid-State Circuits, **2013**, vol. 48 no. 7 pp. 1638-1650.

30. Chitnis D. and Collins. S. "A SPAD-based photon detecting system for optical communications." J. of Lightw. Tech. 2014, vol. 32 no. 10 pp. 2028-2034.
31. Cusini I., Berretta D., Conca E., Incoronato A., Madonini F., Maurina A.A., Nonne C., Riccardo S., and Villa F. "Historical Perspectives, State of Art and Research Trends of SPAD Arrays and Their Applications (Part II: SPAD Arrays)" Frontiers in Physics, **2022**, vol. 10.
32. Morimoto K. et al., "3.2 Megapixel 3D-Stacked Charge Focusing SPAD for Low-Light Imaging and Depth Sensing", 2021 IEEE International Electron Devices Meeting (IEDM), **2021**, pp. 20.2.1-20.2.4.
33. Andreas E., Henderson R., Schmidtke B., Funk T., Grant L., Richardson J., and Freude W."185 MHz count rate 139 dB dynamic range single-photon avalanche diode with active quenching circuit in 130 nm CMOS technology". Proc. Int. Image Sensor Workshop, **2011**, pp. 278-280.
34. Ogi J. et al., "A 124-dB Dynamic-Range SPAD Photon-Counting Image Sensor Using Subframe Sampling and Extrapolating Photon Count", in IEEE Journal of Solid-State Circuits, **2021**, vol. 56, no. 11, pp. 3220-3227.
35. Rimmelspacher J., Werthof A., Weigel R. and Issakov V., "Systematic Experimental f_T and f_{max} Comparison of 40-nm Bulk CMOS versus 45-nm SOI Technology", 2019 14th European Microwave Integrated Circuits Conference (EuMIC), 2019, pp. 200-203.
36. Lindner S., Pellegrini S., Henrion Y., Rae B., Wolf M. and Charbon E., "A High-PDE, Backside-Illuminated SPAD in 65/40-nm 3D IC CMOS Pixel With Cascoded Passive Quenching and Active Recharge", IEEE Electron Device Letters, **2017**, vol. 38, no. 11, pp. 1547-1550.
37. https://eu.mouser.com/pdfDocs/II-VI_Incorporated_12212021_FTLF8536P5xyzSpecificationRevA3.pdf (Accessed on 7 December 2022)